# Soft Matter

## Perpendicular alignment of the phase-separated boundary in adhered polymer droplets

| | |
|---|---|
| Journal: | *Soft Matter* |
| Manuscript ID | SM-ART-08-2021-001180.R1 |
| Article Type: | Paper |
| Date Submitted by the Author: | 14-Sep-2021 |
| Complete List of Authors: | Shinohara, Eriko; Tokyo University of Agriculture and Technology Faculty of Engineering Graduate School of Engineering<br>Watanabe, Chiho; Hiroshima University, Graduate School of Integrated Sciences for Life<br>Yanagisawa, Miho; The University of Tokyo, Basic science |
| | |

## SCHOLARONE™
Manuscripts

# Perpendicular alignment of the phase-separated boundary in adhered polymer droplets

Eriko Shinohara[1,2], Chiho Watanabe[1,3], Miho Yanagisawa[1,4, *]

[1] Komaba Institute for Science, The University of Tokyo, Komaba 3-8-1, Meguro, Tokyo 153-8902, Japan

[2] Department of Applied Physics, Tokyo University of Agriculture and Technology, Naka-cho 2-24-16, Koganei, Tokyo 184-8588, Japan

[3] Graduate School of Integrated Sciences for Life, School of Integrated Arts and Sciences, Hiroshima University, Kagamiyama 1-7-1, Higashi-Hiroshima, Hiroshima 739-8521, Japan.

4 Department of Basic Science, The University of Tokyo, Komaba 3-8-1, Meguro, Tokyo 153-8902, Japan

[*] Author to whom correspondence should be addressed.
M. Y.: myanagisawa@g.ecc.u-tokyo.ac.jp
Keywords: phase transition, microgel, wetting, lipid bilayer, droplet adhesion

**Abstract**

We investigated the effect of the adhered interface on the phase separation pattern using two or three adhered droplets containing a binary solution of poly(ethylene glycol) and gelatin. Under the experimental conditions, single domains of the gelatin-rich phase exhibited partial wetting to the droplet adhered interface (DAI) and nonadhered droplet surface. In the case of isolated spherical droplets, the location of the phase separation interface (PSI) of the domains was completely random owing to spatial symmetry. In the adhered droplets, the random orientation of the PSI was observed when the PSI did not contact the DAI. On the other hand, when the PSI contacted the DAI, the PSI was aligned perpendicular to the DAI. Frequency analysis showed that whether the PSI contacts the DAI is purely stochastic. However, the PSI alignment perpendicular to the DAI increases significantly with three adhered droplets, suggesting that the probability increases with increasing DAI area ratio. We explain this perpendicular pattern by the minimization of the interfacial energy and kinetics with a change in the wetting contact angle. These findings will facilitate the research on the phase separation of polymer solutions inside nonspherical micrometric spaces.

## Introduction

The phase separation of biomolecules in cells has attracted significant attention as a novel mechanism of intracellular dynamic organization with a relationship with diseases[1, 2]. From a thermodynamic perspective, phase separation progresses to minimize the Gibbs free energy via nucleation or spinodal decomposition[3, 4]. The two mechanisms can be observed in cells[5, 6]. The conventional mean-field theory is applicable for a bulk solution with a large volume of μL or larger. However, single cells have a very small volume, from pL to fL. Therefore, it is necessary to verify whether the conventional theory is valid for phase separation even in the small system.

To investigate the phase separation behavior in small systems comparable to cells, artificial cells containing polymer solutions have been investigated. The artificial cells commonly used for such analysis are water-in-oil (W/O) droplets covered with a lipid monolayer membrane (Figure 1), which can be treated as an isolated system because there is no apparent molecular exchange with the outer oil phase. The small volume effect on the phase separation has been studied using polymer solutions confined in capillaries[7-9] and polymer films formed between two plates or on a substrate[10-12]. These are one- to two-dimensional systems in which the surface of the solution is in contact with a solid substrate or air, and the affinity at the surface and the system size such as the film thickness affect the phase separation pattern. The droplets used in this study, on the other hand, are three-dimensional small systems surrounded by a lipid membrane.

For example, when a binary solution consisting of poly(ethylene glycol) (PEG) and gelatin separates into two coexisting phases inside a droplet, the domain of the gelatin-rich phase exhibits two different patterns according to the membrane affinity: complete wetting and partial wetting[13]. These two wetting patterns are observed in various polymer droplets by changing the compositions of the polymer solution[14, 15] and membranes covering the droplets[16-19]. Furthermore, the phase separation of small polymer droplets differs from that of large droplets and bulk solutions with a volume of μL or larger. For example, phase separation of PEG/DNA and PEG/bovine serum albumin (BSA) solutions appeared inside small droplets even when the polymer solution maintained a homogeneous phase in large droplets and bulk systems[20, 21]. These reports show that the phase separation pattern of small polymer droplets is sensitive to the affinity between the polymers and membrane covering the droplets.

In addition to isolated droplets, droplet networks consisting of a large number of droplets also become popular for use as model cell tissue[22-25]. The droplet network is readily prepared by bringing the droplets into contact with each other to form a lipid bilayer. Thus, the droplet network has a flat adhered interface of the lipid bilayer, unlike isolated spherical droplets covered with a lipid monolayer. The spatial asymmetry and local presence of the lipid bilayer

are expected to alter the phase separation pattern of polymer solutions. However, to the best of our knowledge, there are no reports on the phase separation patterns of polymer solutions in adhered droplets.

We investigated the phase separation pattern using two or three adhered droplets in which a single domain in the coexisting liquid–liquid (L–L) phase or liquid–gel (L–G) phase is partially wet on the droplet surface (Figure 1). We chose these two polymer systems because of their physicochemical relevance to the cytoplasm where liquids and gels coexist. The intracellular phase separation is attracting much attention in relation to various biological functions and to diseases[26, 27]. In addition, a wetting transition of the liquid domain to the membrane was reported to occur in autophagy[28]. Therefore, investigating the relationship between phase separation and wetting in a cell-sized space is important for soft matter physics and also for biology. The binary polymer solutions to prepare the coexisting phases are PEG/gelatin and PEG/dextran solutions. Regardless of the polymer composition or coexistence phase, the phase separation interface (PSI) is oriented perpendicular to the droplet adhered interface (DAI) if the PSI contacts the DAI. We explained this configuration by considering the interfacial energy and kinetics with a change in the wetting contact angle. These findings demonstrate a way to regulate the position of partially wetting domains inside droplets by changing the droplet shape and spatial heterogeneity of the interfacial tension. In addition, it should provide a basis for the analysis of the phase separation pattern of polymer solutions inside droplet networks consisting of a large number of droplets[22-25].
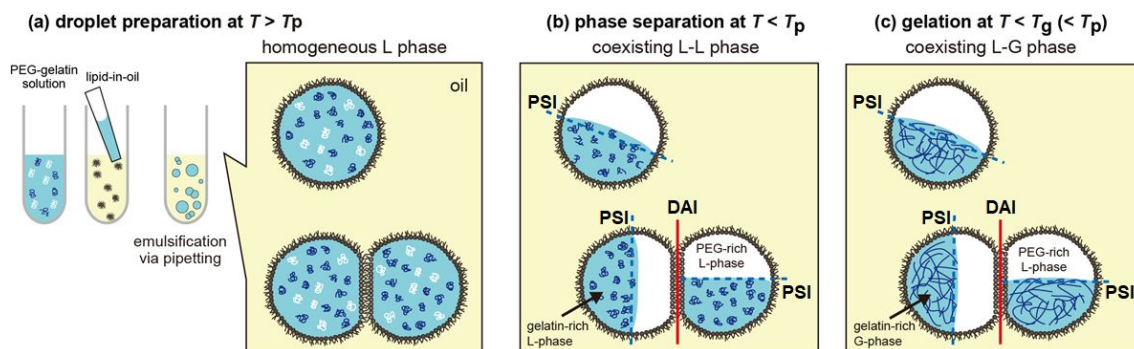


**Fig. 1.** Schematics of two adhered droplets containing a PEG/gelatin solution. With the decrease in temperature $T$, the PEG/gelatin solution transits from (a) a homogeneous L phase to (b) a coexisting L–L phase (at $T$ below the phase transition point, $T_p$) and (c) coexisting L–G phase (at $T$ below the gelation temperature of gelatin, $T_g$). The blue and white regions in (b, c) present gelatin-rich and PEG-rich phases, respectively. The PSI and DAI are shown as a blue dotted line and red solid line, respectively.

**Materials and Methods**

**Materials.**   1,2-dioleoyl-*sn*-glycero-3-phosphocholine   and   PEG   with   a   weight-average molecular weight ($M_w$) of 20,000 were purchased from FUJIFILM Wako Pure Chemical Co. (Tokyo, Japan). 1-Palmitoyl-2-oleoyl-*sn*-glycero-3-phosphocholine (PC) was obtained from NOF Corporation (Tokyo, Japan). Dextran from *Leuconostoc* spp. ($M_w$ = 450,000–650,000) was purchased from Sigma-Aldrich (St. Louis, MO, USA). Alkali-treated gelatin ($M_w$ = 69,000) was purchased from Merck (Darmstadt, Germany). The isoelectric point (IEP) was approximately at a pH of 4.5. For fluorescence observation of the PEG/gelatin system, fluorescein isothiocyanate isomer I (FITC) (Sigma-Aldrich) was used as a fluorescent dye for gelatin. For fluorescence observation of the PEG/dextran system, a FITC-labeled dextran ($M_w$ = 500,000; Sigma-Aldrich) and rhodamine B-labeled PEG (Rho-PEG) ($M_w$ = 5,000; Biochempeg Scientific Inc., Watertown, MA, USA) were used. The samples were then used without further purification. Mineral oil (Nacalai Tesque Inc., Kyoto, Japan) and distilled water (Thermo Fischer Scientific Inc., Waltham, MA, USA) were used to prepare the oil and water phases, respectively. The oils were stored in the presence of molecular sieves to preserve their anhydrous state before droplet preparation.

**PEG/gelatin solution in the bulk.** The polymer composition was fixed to 1.7 wt% PEG and 5.0 wt% gelatin, so that the volume fraction of the two coexisting phases was 1:1[29]. The PEG/gelatin solution was prepared at 70 °C. With the decrease in temperature $T$, the PEG/gelatin system undergoes liquid–liquid phase separation (L–L phase) at $T_p \sim 30$ °C and the gelatin-rich phase transitions to the gel phase below $T_g \sim 27$ °C (L–G phase). The pH of the solution obtained in the L–L phase was closer to the IEP of gelatin.

**PEG/dextran solution in bulk.** The polymer composition was fixed to 6.3 wt% dextran and 1.8 wt% PEG. The PEG/dextran solution was prepared at room temperature (~23 °C). We confirmed that the bulk solution remained in a homogeneous phase.

**Preparation of adhered droplets.** W/O droplets covered with a lipid monolayer were prepared using a reported method[13, 20, 30]. Briefly, dry lipid films were prepared on the bottom of a glass tube. Mineral oil was added to the lipid films before sonication for 90 min at 70 °C (above the transition temperature of the lipid PC). An approximately 1 mM lipid-in-oil solution was prepared and used within a day. Approximately 10 vol% of the PEG/gelatin solution was added to the lipid-in-oil solution, followed by emulsification via pipetting to obtain adhered droplets.

During the pipetting process, some droplets come into contact with each other by chance to form stable two or three adhered droplets. The sample temperature was maintained at ~70 °C ($>T_p$) to prevent L–L phase separation of the PEG/gelatin solution inside the droplets during pipetting. Immediately after the pipetting, an aliquot containing the droplets was placed between two cover glasses with a spacer (thickness: 0.2 mm). For fluorescence microscopy observation, 0.5 wt% of gelatin was replaced with a FITC-conjugated gelatin[13]. The sample temperature was held at 70 °C for 30 min (homogeneous L phase), then lowered from 70 to 30 °C (coexisting L–L phase), and quenched to ~23 °C after another 30 min (coexisting L–G phase). For the PEG/dextran droplet preparation, we prepared the adhered droplets in the same manner at room temperature (~23 °C) because the PEG/dextran bulk solution maintained a homogeneous L phase at room temperature. In the observation of the droplets using fluorescence microscopy, FITC-dextran and Rho-PEG were mixed with the dextran and PEG solutions with a final concentration of each fluorophore of 0.1 mg/mL, respectively. We confirmed the presence of lipid monolayer at the droplet surface and lipid bilayer at the DAI by image analysis using fluorescently labeled lipids and molecular transport activity through reconstituted membrane protein nanopores, respectively[22, 31].

**Fluorescence microscopy observations.** For the PEG/gelatin system, confocal laser-scanning microscopy (Olympus IX83 with FV1200, Olympus, Tokyo, Japan) was used to observe the phase separation inside the droplets. The FITC-labeled gelatin was excited at 473 nm by a laser and the emission was collected in the range of 490–590 nm. The pinhole size was fixed at approximately 1 μm. For the PEG/dextran system, a fluorescent microscope (Olympus IX 73, Olympus) equipped with a Hg lamp was used to observe phase separation. The emissions of FITC-dextran and Rho-PEG were collected in the ranges of 510–550 nm and 575–625 nm, respectively. The obtained images were analyzed by the National Institutes of Health (NIH) Image J software. Most of the fluorescent images shown here were acquired along the equatorial plane of two or three adhered droplets with similar radii.

**Interfacial tension measurement**

The interfacial tensions between the coexisting polymer phases (PEG/gelatin interface) and between the polymer phase (PEG or gelatin phase) and DAI were evaluated using a contact angle analysis[14]. In addition, the surface tension of the polymer droplets covered with a lipid monolayer was measured using the pendant drop method (DM-501, Kyowa Interface Science Co., Saitama, Japan).

**3. Results and Discussions**

**Phase separation patterns in the two or three adhered droplets**

We analyzed the characteristics of the phase separation patterns of binary polymer solutions inside the adhered droplets. Figures 2a–c show examples of two adhered droplets where the binary polymer solution of PEG/gelatin is confined inside. In the fluorescence images, the single domain of the gelatin-rich G phase is shown in white. The PSI and DAI are marked with a blue dotted line and red solid line in the schematic (Figure 2d). Focusing on the positional relationship between the PSI and DAI, the PSI appears to be perpendicular to the DAI (Figure 2a) or, in some cases, not perpendicular to the DAI (Figure 2c). The position of PSI with respect to DAI was not always the same for each of the two adhered droplets. In the case in Figure 2b, the perpendicular position of the PSI was observed in only one of the two droplets.

To reveal the positional relationship between the PSI and DAI, we classified the patterns by considering the combination of the PSI edge positions and gelatin-rich phase (blue in the schematic). As shown in Figure 2e, there are seven possible patterns for the two adhered droplets. In the case of nonperpendicular patterns, the PSI edge is not in contact with the DAI (i–iii). On the other hand, at least one of the PSI edges is in contact with the DAI for perpendicular patterns (iv, v). The other cases are mixed patterns of the two (vi, vii). Therefore, perpendicular or nonperpendicular patterns can be represented as patterns of PSI with and without DAI contact.

Based on the classification of Figure 2e, we counted the pattern frequency, as shown in Figure 2f. The patterns of (i), (iv), (v), and (vi) are more frequent than those of (ii), (iii), and (vii). This clearly shows that the pattern of DAI fully covered by the gelatin-rich phase is unfavorable. In addition, the PSI pattern in contact with the DAI (perpendicular pattern) is widely observed in the patterns of (iv), (v), and (vi). However, the most frequent pattern is the mixed pattern (vi), and the second most frequent pattern is not both PSI perpendicular patterns (iv, v) but both PSI parallel pattern (i) against the DAI. The frequency of (i) is 27, and the sum of the frequencies of (iv) and (v) is 30, almost the same value. This result suggests that the probability of PSI contacting the DAI is almost 50%. It is also supported by the fact that the mixed pattern is the most frequent. The probability of the PSI contacting the DAI is expected to increase as the DAI area increases. To testify the idea, we next analyzed the phase separation patterns for three adhered droplets, with a larger adhered area than the two adhered droplets.
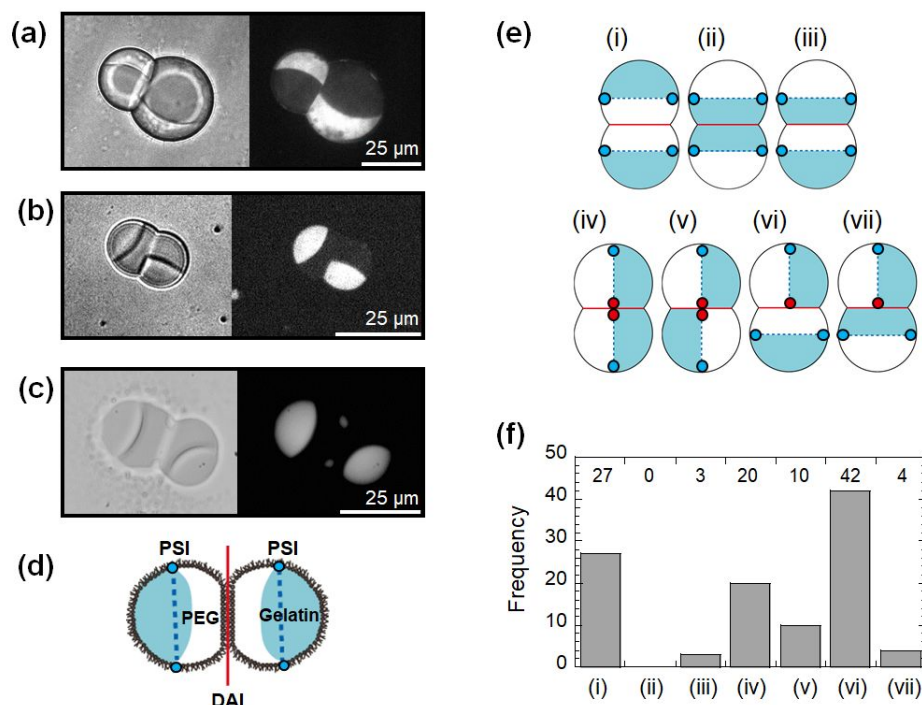
**Fig. 2.** Phase separation patterns of the gelatin/PEG solution in two adhered droplets. (a–c) Transmission images (left) and fluorescence images (right). The two coexisting phases are the PEG-rich L phase and gelatin-rich G phase (shown in white in the fluorescence images). (d) Schematic of (c). The PSI and DAI are shown as blue dotted lines and red solid lines, respectively. (e) Possible patterns having different PSI edge positions: PSI contact with the DAI (i–iii), without contact (iv, v), and mix of the two cases (vi, vii). The red and blue points indicate the PSI edges with and without DAI contact, respectively. (f) Histogram of the observed patterns classified according to (e). The total number of two adhered droplets used in the analysis, $N$ is 106.

Figure 3 shows such examples where the three droplets are arranged in a row. Surprisingly, unlike the two adhered droplets, only a perpendicular pattern with PSI contacting the DAI was observed for the three adhered droplets. The perpendicular pattern occurs not only in the central droplet with a high DAI area ratio but also in the droplets at both ends. This result supports our idea that the probability of the PSI contacting DAI increases as the DAI increases. However, the frequency cannot be statistically analyzed because it is challenging to prepare a large number of three adhered droplets. Furthermore, we analyzed such phase separation patterns using a different polymer system of the PEG/dextran solution (Figures 3d–e). In the fluorescence images (right), the PEG-rich L phase and dextran-rich L phase are shown in red and green, respectively. Similar to the three adhered droplets containing the PEG/gelatin solution,

perpendicular patterns were observed. When the dextran-rich phase in the PEG/dextran system corresponds to the gelatin-rich phase in the PEG/gelatin system, the patterns in Figures 3d and 3e correspond to the patterns in Figures 2e (iv) and (v). These results support our claim that the whether the PSI contacts DAI is a stochastic process and PSI perpendicular position to the DAI becomes more favorable as the DAI area increases via droplet adhesion.
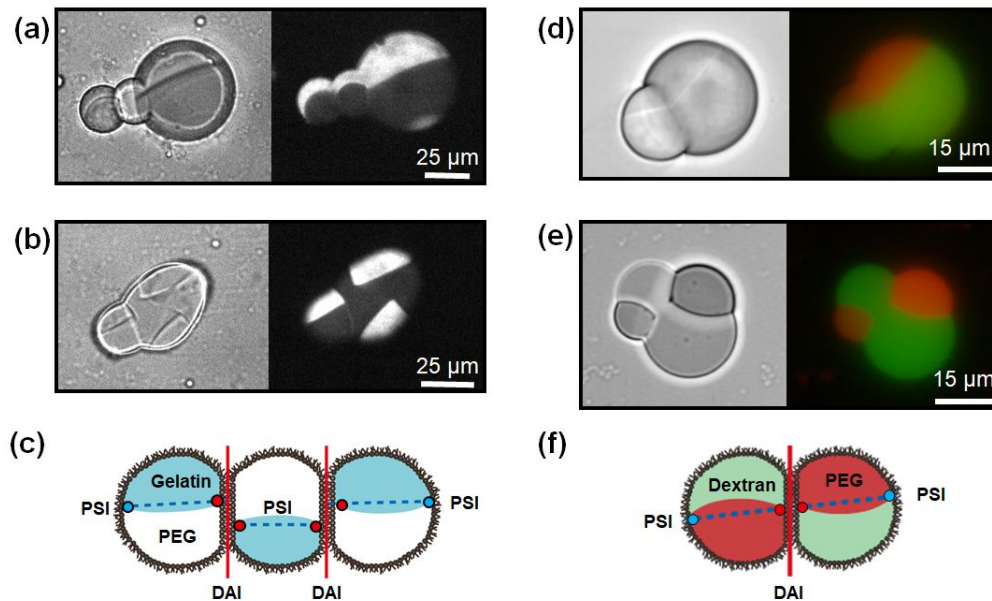


**Fig. 3.** Phase separation patterns in three adhered droplets of the PEG/gelatin solution and in two adhered droplets of the PEG/gelatin solution. (a-b, d–e) Transmission images (left) and fluorescence images (right). (a, b) The gelatin-rich G phase is shown in white. (d–e) PEG-rich and dextran-rich L phases are shown in red and green, respectively. (c, f) Schematics of (b, e), respectively. The DAI and PSI are shown as red solid lines and blue dotted lines, respectively. The red and blue points indicate the PSI edges in and not in contact with the DAI, respectively.

**Independent droplet analysis of domain position against the DAI**

So far, the pattern has been analyzed for the adhered droplet pair, but here, each droplet was analyzed independently to make clear why the PSI aligns perpendicular to the DAI when it comes into contact with the DAI. We analyzed the positions of the PSI edge and gelatin-rich domain, as well as the angle $\theta_p$ between the PSI line (connecting the PSI edges indicated by the points) and DAI line for the two adhered droplets containing the PEG/gelatin solution (Figure 4a). As suggested by the paired analysis (Figure 2f), the PSI contacting the DAI (perpendicular pattern) and not contacting the DAI (parallel pattern) occur with equal probability, and in the parallel pattern, the PEG-rich phase covers the DAI (Figure 4b). Histograms of the PSI angle $\theta_p$ are shown for droplets according to the presence/absence of contact of the PSI edges with the

DAI (Figures 4c, d). In the case of PSI in contact with the DAI (Figure 4c), the PSI angle $\theta_p$ has an apparent peak in the range of 90° to 110°, which confirmed that the PSI is arranged perpendicular to the DAI. On the other hand, for PSI that was not in contact with the DAI, there were no apparent peaks in the histogram (Figure 4d). These results demonstrate that, when the PSI is in contact with the DAI, the PSI arranges perpendicular to the DAI. On the contrary, if the PSI is not in contact with the DAI, the PSI position is random, as in the case of isolated spherical droplets. This shows that not only the presence of DPI but also the PSI edge in contact with DPI is needed to align the PSI position.
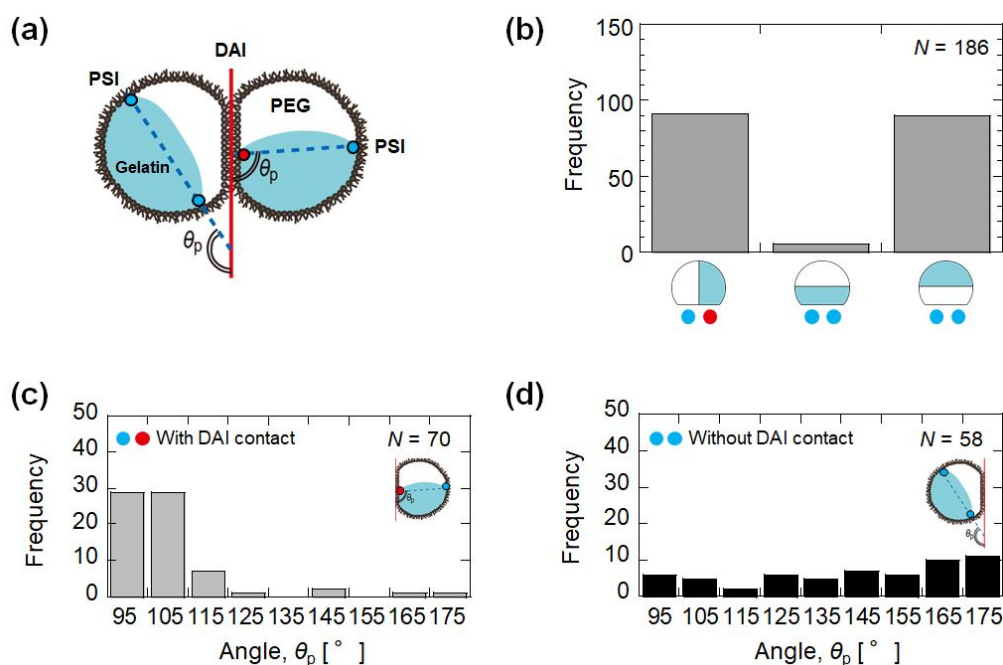


**Fig. 4.** PSI position against the DAI. (a) Definition of the PSI position with or without DAI contact and PSI angle $\theta_p$ between the PSI line (blue dotted line, connecting both PSI edges (indicated by points)) and DAI line (red solid line). $\theta_p$ is set to be >90°. (b) Histogram of the PSI location with or without PSI contact and PEG-rich phase location facing DAI or not facing it. (c, d) Histograms of $\theta_p$ for droplets where the PSI edges are (c) in and (d) not in contact with DAI.

**Droplet shape and PSI curvature**

When PSI was in contact with the DAI, the phase separation pattern changed and the PSI was aligned perpendicularly to the DAI (Figure 4c). In addition, the gelatin-rich domain in the two

adhered droplets was away from the DAI (Figures 2f, 4b). We explain the above two features of the phase separation pattern for two adhered droplets by a free energy analysis.

First, we analyze the geometrical configuration, *i.e.*, whether the morphological difference of the adhered droplets according to the PSI position to the DAI is negligible. This is important because, if it is negligible, we only need to consider the free energies of the confined polymers. By elliptical fitting, we obtain the histograms of the axis ratio *a*/*b*, where the length perpendicular to the DAI is *a*, while the axis parallel to the DAI is *b* (Figure 5a). Considering the most frequent value (mode value), the axis ratio of *a*/*b* is approximately 0.99 for perpendicular patterns with DAI contact and 1.01 for nonperpendicular patterns without DAI contact. However, the difference was within the standard error bars. Therefore, we concluded that there is a negligible correlation between the droplet shape and PSI position. In the following analysis, we consider only the contributions of the confined polymer solution inside the adhered droplets.

Second, we focused on the PSI curvature. For the PEG/gelatin system, the interfacial energy between the two coexisting phases dominates the free energy, and thus the domain exhibits a dewetting transition[13]. This implies that a smaller interfacial area between the PEG-rich phase and gelatin-rich phase leads to a lower free energy of the droplet. The interfacial area can be minimized by reducing the axial length of the droplet along with the PSI and setting the curvature of the PSI to zero. Therefore, we used a PSI curvature analysis to estimate whether the PSI perpendicular pattern is energetically more advantageous.

The PSI curvature analysis was performed using the ratio between the PSI length (along the phase boundary), $l_{p1}$, and length connecting the PSI edges, $l_{p2}$ (Figure 5b, left). When $l_{p1} = l_{p2}$, the PSI curvature is almost zero, and thus the interfacial energy of the PSI is minimized. The difference in the mean value of $l_{p1}/l_{p2}$ between the two patterns is within the standard error bar, but the mode value for the PSI in contact with the DAI (left) is closer to 1 than that without contact with the DAI (right). Hence, the perpendicular pattern of the PSI in contact with the DAI is likely to occur due to the minimization of the interfacial energy acting on the PSI.
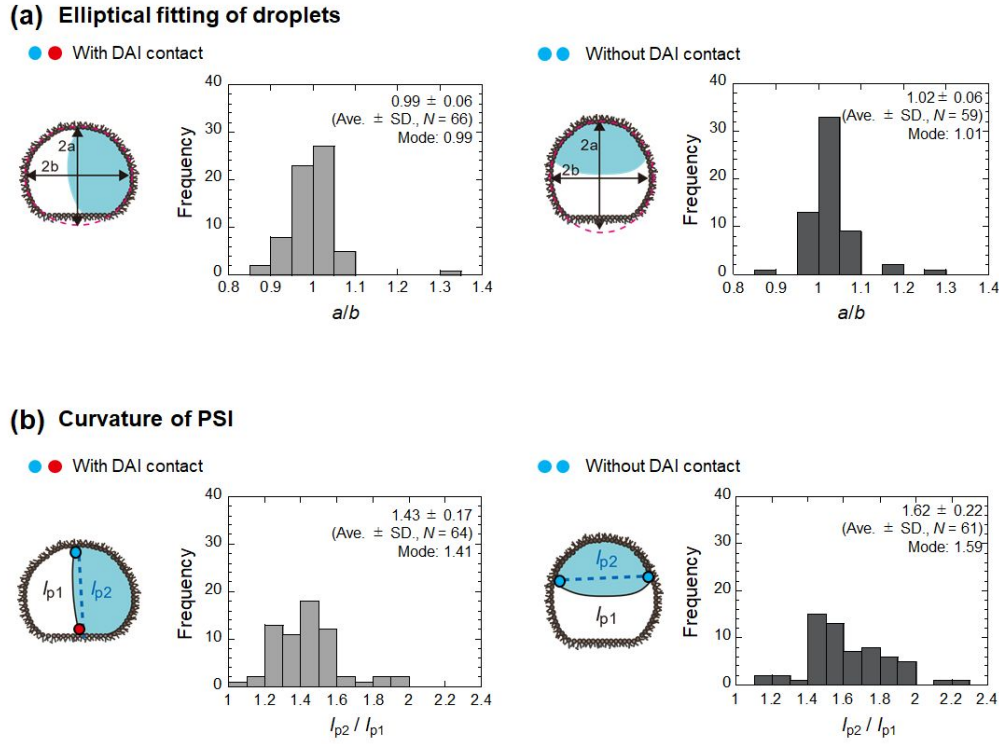
**Fig. 5.** (a) Elliptical shape analysis of the droplets. *a/b* is the axial ratio of the parallel axis to the vertical axis against the DAI. (b) Curvature analysis of the PSI. $l_{p1}$ is the length of the interfacial curve (black solid line), while $l_{p2}$ is a point-to-point line of the interface edge on the membrane (blue dotted line).

**Interfacial energy analysis**

To investigate whether the PSI perpendicular position to the DAI is energetically advantageous among others, we calculated the free energy of the droplets with different PSI positions using the values of interfacial tensions. Notably, the droplet shape was approximately spherical regardless of the PSI patterns, as explained above (Figure 5a). Therefore, in the following analysis, we ignored the morphological changes according to the PSI positions.

The gelatin-rich domain can exhibit two different contact angles, wetted to the nonadhered droplet surface $\theta_{og}$ and DAI $\theta_{mg}$ (Figure 6a). These contact angles should be balanced by three different interfacial tensions. For the contact angle $\theta_{og}$ (> 90°), the cosine approximately obeys the Young's equation on a flat surface[14, 32],

$$\gamma_{op} = \gamma_{og} - \gamma_{pg}\cos\theta_{og} \#(1)$$

where $\gamma_{pg}$ and $\gamma_{oi}$ (i = p, g) are the interfacial tensions between the coexisting polymer phases (PEG-rich and gelatin-rich phases) and between each polymer phase and droplet surface, respectively. Using the pendant drop method, we obtained $\gamma_{og}$ = 1.6 mN/m and $\gamma_{op}$ = 3.5 mN/m. In addition, $\theta_{og}$ was 109 ± 3° (N = 44, average ± standard error (SE), Figure 6b). By substituting

these values into Equation (1), we can estimate $\gamma_{pg}$ as ~5.8 mN/m. This estimated $\gamma_{pg}$ larger than $\gamma_{op}$ and $\gamma_{og}$ is reasonable because experimentally the gelatin-rich domain inside isolated droplets exhibits a dewetting transition, which implies that $\gamma_{pg} > \gamma_{op}$ and $\gamma_{og}$[13].
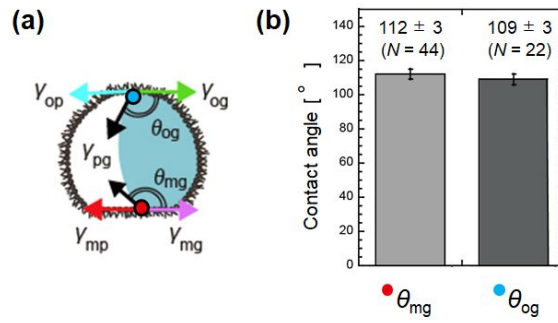


**Fig. 6.** Contact angles for the gelatin-rich domain inside the droplets (average ± SE). (a) Definitions of the interfacial tensions between the droplet surface and coexisting polymers (*i.e.,* PEG-rich or gelatin-rich phase) $\gamma_{oi}$ (i = p or g), between the respective polymer phase and DAI $\gamma_{mi}$ (i = p or g), and between the coexisting polymer phases $\gamma_{pg}$. (b) The contact angles of $\theta_{og}$ and $\theta_{mg}$ denote the angles between the domain and droplet surface (indicated by the blue point) and DAI (indicated by the red point), respectively.

Similarly, we estimate the magnitude relationship between $\gamma_{mg}$ and $\gamma_{mp}$ as follow,

$$\gamma_{mp} = \gamma_{mg} - \gamma_{pg}\cos\theta_{mg}, \#(2)$$

where $\gamma_{mi}$ (i = p, g) is the interfacial tension between the polymer phase and DAI. By substituting the values of $\theta_{wg}$ and $\gamma_{pg}$, we obtain the relationship $\gamma_{mg} = \gamma_{mp} + 2.2$ mN/m. This implies that the interfacial tension of the PEG-rich phase on the DAI is smaller than that of the gelatin-rich phase, $\gamma_{mg} > \gamma_{mp}$. This magnitude relationship seems to have an opposite trend of the membrane affinity compared to the droplet surface ($\gamma_{og} < \gamma_{op}$). However, for the PEG/dextran solution inside lipid bilayer liposomes, likely to the DAI, $\gamma_{mp}$ also has a smaller value than that between the dextran-rich phase and lipid bilayer[33]. Therefore, the interfacial tension between the polymer solution and membrane may be sensitive to the membrane property, *i.e.*, the lipid monolayer at the droplet surface or lipid bilayer at the DAI. The derived magnitude relationships of $\gamma_{mg} > \gamma_{mp}$ and $\gamma_{og} < \gamma_{op}$ demonstrate that the PEG-rich phase preferentially covers the DAI, not the gelatin-rich phase, to minimize the interfacial energy. In addition, the most dominant interfacial tension was $\gamma_{pg}$.

Finally, we compared the interfacial energy of the perpendicular pattern to the nonperpendicular-pattern DAI fully covered by the PEG-rich phase. In the case of two adhered

droplets, each pattern occurred eventually, but, in the case of three adhered droplets, only perpendicular patterns appeared (Figure 3). With the increase in the DAI, $\gamma_{pg}$ at the PSI dominates the total interfacial energy. Because the PSI surface area of the perpendicular pattern is geometrically smaller than that of the nonperpendicular pattern, the perpendicular pattern becomes more stable (Figure 7a). Furthermore, if the PSI does not move to a perpendicular position after the PSI edge touches the DAI, the contact angle of the gelatin-rich domain on the DAI $\theta_{mg}$ cannot have a stable angle. This is different from the contact angle on the nonadhered droplet surface $\theta_{og}$; i.e., both ends can have a stable angle regardless of the domain position (Figure 7b). This difference in the contact angle of the wetting domain upon migration is responsible for the PSI angle of the perpendicular pattern of ~90°, while the PSI angle of the nonperpendicular pattern is random (Figure 4).



**Fig. 7.** Possible mechanism of the PSI edge pinned at the DAI after the DAI contact. Differences in the contact angle according to the position of the gelatin-rich domain (glue) (a) with and (b) without DAI contact.

**Conclusions**

We analyzed the effect of the adhered interface on the phase separation pattern using two or three adhered droplets of the PEG/gelatin solution. The position of the phase separation boundary in the adhered droplets had the following three characteristics, unlike in the isolated spherical droplets. (i) The PEG-rich phase preferred the DAI rather than a nonadhered droplet surface. (ii) When the PSI contacted the DAI, the PSI oriented perpendicularly to the DAI. (iii) On the other hand, when the PSI did not contact the DAI, the PSI position was not correlated with the DAI (random orientation). These characteristics of the phase separation pattern were explained by considering the kinetic process with changes in the wetting contact angle and interfacial energy. These findings will facilitate the research on the phase separation of polymer solutions inside droplet networks[22-25] and adhered liposomes[34, 35] that advances biophysics and soft matter physics using small volume of a polymer solutions. In addition, this information will be useful for the preparation of nonspherical microgels upon polymerization of adhered polymer droplets after phase separation[13, 36, 37]. This can be established as a new method for preparing non-spherical microgels by adhering phase-separated droplets to each other prior to

13

polymerization. As with non-spherical colloids[38], it will also be able to trap small particles in their dents and form aggregates according to their shape. Furthermore, various molecular behaviors such as sol–gel transition (gelation)[31, 39, 40], molecular diffusion[20, 30, 41], biochemical reactions[42], and reaction-diffusion waves[43] are different in small droplets from those in the corresponding bulk systems. Therefore, these molecular behaviors are also expected to be altered upon droplet adhesion and should be investigated in the near future.

## Conflicts of interest

There are no conflicts to declare.

## References

1.      Y. Shin and C. P. Brangwynne, *Science*, 2017, **357**, eaaf4382.
2.      S. Alberti and A. A. Hyman, *Nat. Rev. Mol. Cell Bio.*, 2021, **22**, 196-213.
3.      R. Shimizu and H. Tanaka, *Nat. Commun.*, 2015, **6**, 7407.
4.      A. A. Hyman, C. A. Weber and F. Julicher, *Annu. Rev. Cell. Dev. Biol.*, 2014, **30**, 39-58.
5.      D. Bracha, M. T. Walls, M. T. Wei, L. Zhu, M. Kurian, J. L. Avalos, J. E. Toettcher and C. P. Brangwynne, *Cell*, 2019, **176**, 407-407.
6.      J. Berry, S. C. Weber, N. Vaidya, M. Haataja and C. P. Brangwynne, *Proc. Natl. Acad. Sci. U. S. A.*, 2015, **112**, E5237-5245.
7.      H. Tanaka, *Phys Rev Lett*, 1993, **70**, 53-56.
8.      H. Tanaka, *Phys Rev Lett*, 1993, **70**, 2770-2773.
9.      H. Tanaka, *Journal of Physics: Condensed Matter*, 2001, **13**, 4637-4674.
10.     K. Tanaka, A. Takahara and T. Kajiyama, *Macromolecules*, 1996, **29**, 3232-3239.
11.     N. Bhandaru, A. Karim and R. Mukherjee, *Soft Matter*, 2017, **13**, 4709-4719.
12.     A. Das, A. B. Dey, S. Chattopadhyay, G. De, M. K. Sanyal and R. Mukherjee, *Langmuir*, 2020, **36**, 15270-15282.
13.     M. Yanagisawa, S. Nigorikawa, T. Sakaue, K. Fujiwara and M. Tokita, *Proc. Natl.*

*Acad. Sci. U. S. A.*, 2014, **111**, 15894-15899.

14. Y. H. Li, R. Lipowsky and R. Dimova, *J. Am. Chem. Soc.*, 2008, **130**, 12252-+.

15. Q. Zhang, M. Xu, X. Liu, W. Zhao, C. Zong, Y. Yu, Q. Wang and H. Gai, *Chem Commun (Camb)*, 2016, **52**, 5015-5018.

16. M. Andes-Koback and C. D. Keating, *J. Am. Chem. Soc.*, 2011, **133**, 9545-9555.

17. S. Botterbusch and T. Baumgart, *Appl Sci-Basel*, 2021, **11**.

18. C. D. Keating, *Accounts of chemical research*, 2012, **45**, 2114-2124.

19. L. D. Zarzar, V. Sresht, E. M. Sletten, J. A. Kalow, D. Blankschtein and T. M. Swager, *Nature*, 2015, **518**, 520-524.

20. C. Watanabe, Y. Kobori, J. Yamamoto, M. Kinjo and M. Yanagisawa, *J Phys Chem B*, 2020, **124**, 1090-1098.

21. N. Biswas, M. Ichikawa, A. Datta, Y. T. Sato, M. Yanagisawa and K. Yoshikawa, *Chem Phys Lett*, 2012, **539**, 157-162.

22. S. Fujiwara, K. Shoji, C. Watanabe, R. Kawano and M. Yanagisawa, *Micromachines-Basel*, 2020, **11**.

23. F. Del Giudice, G. D'Avino and P. L. Maffettone, *Lab Chip*, 2021, **21**, 2069-2094.

24. A. Alcinesio, O. J. Meacock, R. G. Allan, C. Monico, V. Restrepo Schild, I. Cazimoglu, M. T. Cornall, R. Krishna Kumar and H. Bayley, *Nat. Commun.*, 2020, **11**, 2105.

25. V. M. Gaspar, P. Lavrador, J. Borges, M. B. Oliveira and J. F. Mano, *Advanced materials*, 2020, **32**, e1903975.

26. A. Patel, H. O. Lee, L. Jawerth, S. Maharana, M. Jahnel, M. Y. Hein, S. Stoynov, J. Mahamid, S. Saha, T. M. Franzmann, A. Pozniakovski, I. Poser, N. Maghelli, L. A. Royer, M. Weigert, E. W. Myers, S. Grill, D. Drechsel, A. A. Hyman and S. Alberti, *Cell*, 2015, **162**, 1066-1077.

27. Y. Shin and C. P. Brangwynne, *Science*, 2017, **357**.

28. J. Agudo-Canalejo, S. W. Schultz, H. Chino, S. M. Migliano, C. Saito, I. Koyama-Honda, H. Stenmark, A. Brech, A. I. May, N. Mizushima and R. L. Knorr, *Nature*, 2021, **591**, 142-146.

29. M. Yanagisawa, Y. Yamashita, S.-a. Mukai, M. Annaka and M. Tokita, *J. Mol. Liq.*, 2014, **200**, 2-6.

30. K. Harusawa, C. Watanabe, Y. Kobori, K. Tomita, A. Kitamura, M. Kinjo and M. Yanagisawa, *Langmuir*, 2021, **37**, 437-444.

31. A. Sakai, Y. Murayama, K. Fujiwara, T. Fujisawa, S. Sasaki, S. Kidoaki and M. Yanagisawa, *ACS. Cent. Sci.*, 2018, **4**, 477-483.

32. R. Lipowsky, *J Phys Chem B*, 2018, **122**, 3572-3586.

33. Y. H. Li, H. Kusumaatmaja, R. Lipowsky and R. Dimova, *J Phys Chem B*, 2012, **116**,

1819-1823.

34.     A. Oda, C. Watanabe, N. Aoki and M. Yanagisawa, *Soft Matter*, 2020, **16**, 4549-4554.

35.     D. T. Gonzales, C. Zechner and T. Y. D. Tang, *Current Opinion in Systems Biology*, 2020, **24**, 56-63.

36.     C. H. Choi, D. A. Weitz and C. S. Lee, *Advanced materials*, 2013, **25**, 2536-2541.

37.     Q. Ma, Y. Song, W. Sun, J. Cao, H. Yuan, X. Wang, Y. Sun and H. C. Shum, *Adv. Sci.*, 2020, **7**, 1903359.

38.     S. Sacanna, W. T. M. Irvine, P. M. Chaikin and D. J. Pine, *Nature*, 2010, **464**, 575-578.

39.     A. Sakai, Y. Murayama and M. Yanagisawa, *Langmuir*, 2020, **36**, 5186-5191.

40.     M. Yanagisawa, C. Watanabe and K. Fujiwara, *Gels*, 2018, **4**, 29.

41.     C. Watanabe and M. Yanagisawa, *Phys. Chem. Chem. Phys.*, 2018, **20**, 8842-8847.

42.     A. Kato, M. Yanagisawa, Y. T. Sato, K. Fujiwara and K. Yoshikawa, *Sci. Rep.*, 2012, **2**, 283.

43.     S. Kohyama, N. Yoshinaga, M. Yanagisawa, K. Fujiwara and N. Doi, *Elife*, 2019, **8**.